OPEN ACCESS



Heliospheric Diffusion of Stochastic Parker Spirals in Radially Evolving Solar Wind Turbulence

N. H. Bian ¹ , R. D. Strauss^{2,3} , G. Li⁴ , and N. E. Engelbrecht^{2,3}
¹ CSPAR, University of Alabama in Huntsville, Huntsville, AL, USA; nbian@hotmail.com

² Center for Space Research, North-West University, Potchefstroom, South Africa

³ National Institute for Theoretical and Computational Sciences NITheCS, South Africa

⁴ Department of Space Sciences and CSPAR, University of Alabama in Huntsville, Huntsville, AL, USA; gangli.uahuntsville@gmail.com

**Received 2023 March 20; revised 2023 November 11; accepted 2023 December 31; published 2024 February 20

Abstract

We present a stochastic field line mapping model where the interplanetary magnetic field lines are described by a density distribution function satisfying a Fokker–Planck equation that is solved numerically. Due to the spiral geometry of the nominal Parker field and to the evolving nature of solar wind turbulence, the heliospheric diffusion of the magnetic field lines is both heterogeneous and anisotropic, including a radial component. The longitudinal distributions of the magnetic field lines are shown to be close to circular Gaussian distributions, although they develop a noticeable skewness. The magnetic field lines emanating from the Sun are found to differ, on average, from the spirals predicted by Parker. Although the spirals remain close to Archimedean, they are here underwound, on average. Our model predicts a spiral angle that is smaller by \sim 5° than the Parker spiral angle at Earth's orbit for the same solar wind speed of $V_{\rm sw}=400~{\rm km~s}^{-1}$. It also predicts an angular position on the solar disk of the best magnetically connected footpoint to an observer at 1 au that is shifted westward by \sim 10° with respect to the Parker's field model. This significantly changes the angle of the most probable magnetic connection between possible sources on the Sun and observers in the inner heliosphere. The results have direct implications for the heliospheric transport of "scatter-free" electrons accelerated in the aftermath of solar eruptions.

Unified Astronomy Thesaurus concepts: Interplanetary turbulence (830); Interplanetary magnetic fields (824)

1. Introduction

Understanding the transport of charged particles accelerated to suprathermal energies in turbulent astrophysical plasma has been a subject of a long endeavor beginning with the work of Fermi (1949) on the production of cosmic rays and its adaptation by Parker & Tidman (1958) to solar flares. The elucidation of the mechanisms responsible for solar energetic particle (SEP) events (Reames 1999; Cliver 2000) remains among the common objectives of the two recently launched Parker Solar Probe and Solar Orbiter missions (McComas et al. 2019; Rodríguez-Pacheco et al. 2020). In addition to the fleet of spacecraft orbiting the Sun, these missions provide an unprecedented source of in situ multipoint measurements of SEP events and remote stereoscopic observations of their sources at the Sun. An important transport process is cross-field diffusion resulting from the interactions between the highenergy particles and the turbulent magnetic fields (Jokipii 1966). This transport process is equally important for precipitating energetic particles, and it can be diagnosed remotely from hard X-ray spectroscopic imaging of flaring coronal loops (Bian et al. 2011; Kontar et al. 2011).

As pointed out originally by Jokipii & Parker (1969), due to fluctuations in the solar wind magnetic fields, the Parker spirals are stochastic. Following the terminology introduced by Bian & Li (2021), we call them stochastic Parker spirals. On the basis of the Leighton (1964) model of magnetic flux diffusion on the photosphere, Jokipii & Parker (1969) developed a boundary-driven model for the angular diffusion of magnetic

Original content from this work may be used under the terms of the Creative Commons Attribution 4.0 licence. Any further distribution of this work must maintain attribution to the author(s) and the title of the work, journal citation and DOI.

field lines in the heliosphere, providing a sound explanation for the angular spread of solar cosmic rays (Meyer et al. 1956) observed by the Pioneer missions (Fan et al. 1968). Since then, the angular dispersion of SEPs has remained an active subject of investigation, in both longitude (Van Hollebeke et al. 1975; Cane et al. 1986; Shea & Smart 1990; Reames 1999; Lario et al. 2006; Mewaldt et al. 2013; Reames et al. 2013; Wiedenbeck et al. 2013; Dröge et al. 2014; Dresing et al. 2014; Richardson et al. 2014; Cohen et al. 2017) and latitude (Zhang et al. 2001; Dalla et al. 2003; Zhang et al. 2003). The statistical analysis of Cohen et al. (2017) shows that the longitudinal widths of SEPs are weakly dependent on the charge-to-mass ratio, suggesting that the angular dispersion of the suprathermal particles is determined by the angular dispersion of the magnetic field line as anticipated by Jokipii & Parker (1969).

In the works of Jokipii & Parker (1969) and Bian & Li (2021, 2022a), the stochastic Parker spirals are described by a stochastic process. This stochastic process is the spherical diffusion process $[\theta(r), \phi(r)]$ for the two heliographic angles, the latitude and the longitude, as a function of the radial distance r from the Sun. The spherical diffusion is superimposed onto the secular longitudinal drift due to the solar rotation. The solutions of the drift diffusion equation governing the longitudinal distribution functions are given by circular Gaussian distributions. There is no radial diffusion of the magnetic field lines in the stochastic Parker spiral model elaborated by Jokipii & Parker (1969) and expanded by Bian & Li (2021, 2022a). The reason is that there is no source of radial magnetic field fluctuations in the boundary-driven model of Jokipii & Parker (1969), which is based on the model of Leighton (1964), where the motions of the magnetic footpoints are described by the spherical drift diffusion process $[\theta(t), \phi(t)]$.

The relation between the two processes, footpoint diffusion on the photosphere and magnetic field line diffusion in the heliosphere, is simply given by $r = r_0 + V_{sw}t$ —the very same relation that applies without consideration for the turbulent diffusion of the magnetic footpoints, as in the case of the Parker spirals. It is the reason that the boundary-driven stochastic Parker spirals of Jokipii & Parker (1969) can be constructed solely from an angular diffusion process with a constant angular diffusivity that is given by the angular diffusivity of the footpoints divided by the solar wind speed and that the process does not involve any radial diffusion of the magnetic field lines. However, due to the spiral geometry of the Parker (1958) field and to the evolving nature of in situ solar wind turbulence, the heliospheric diffusion of magnetic field lines is generally both heterogeneous and anisotropic. The diffusion process also includes a radial component resulting from the presence of radial magnetic field fluctuations in the solar wind. The turbulent structure of the magnetic field lines, on global heliospheric scales, is thus more accurately described by a Fokker-Planck equation with a radially dependent field line diffusion tensor D_m possessing both radial and off-diagonal components, in addition to its purely angular components. These properties lead to unexpected twists in the plot originally elaborated by Jokipii & Parker (1969) and expanded by Bian & Li (2021, 2022a).

In Section 2, we extend the diffusive description of magnetic field lines from local to global scales in the inner heliosphere, taking into account its inhomogeneous and anisotropic properties. In Section 3, the results of numerical simulations of the Fokker–Planck equation describing the turbulent dispersion of the magnetic field lines in the solar wind are presented. In Section 4, an analytic circular Gaussian model for the longitudinal spread of the magnetic field lines around their mean is discussed and compared with the numerical results. A summary of the results and a conclusion are given in Section 5.

2. From Local to Global Diffusion of Magnetic Field Lines in the Solar Wind

We are interested in the turbulent dispersion of magnetic field lines emanating from the Sun and diffusing into the heliosphere. The magnetic field lines are the curves everywhere tangent to the magnetic field at a given time. They are often called the lines of force in reference to their ability to guide the direction of the motions of low-rigidity charged particles. We are interested in both the dispersion of the magnetic field lines and the dispersion of particles propagating at a constant speed along the magnetic field lines in the heliosphere. The equations for the magnetic field lines can be derived from the equations of motion for charged particles interacting with magnetic fields in the limit where the gyroradius of the particles tends to zero. The Lagrangian of a charged particle is given by

$$L = \frac{1}{2}m\mathbf{v}^2 - \left(q\Phi(\mathbf{r},t) - \frac{q}{c}A(\mathbf{r},t)\cdot\mathbf{v}\right),\tag{1}$$

where $A(\mathbf{r}, t)$ is the magnetic vector potential and $\Phi(\mathbf{r}, t)$ is the electric potential. The particle trajectories are determined by extremizing the action (Feynman 1963)

$$\delta \int Ldt = 0. (2)$$

The kinetic energy of the particle is constrained to be conserved outside spatially localized acceleration regions near the Sun, a

condition that is satisfied when the electric potential $\Phi=0$. From the Euler–Lagrange equations for a massless particle, with zero gyroradius, we have that

$$\mathbf{v} \times \nabla \times \mathbf{A}(\mathbf{r}) = 0, \tag{3}$$

an equation that is, by construction, independent of the charge and the mass of the particle. Equation (3) is the magnetic field line equation. It follows that the magnetic field lines are obtained from a variational principle that consists in extremizing the action (Morozov & Solov'ev 1966; Cary & Littlejohn 1983; Elsasser 1986)

$$\delta \int_{r_0}^{r_1} \mathbf{A} \cdot d\mathbf{r} = 0. \tag{4}$$

In other words, the magnetic field line that joins the spatial points \mathbf{r}_0 and \mathbf{r}_1 is obtained from all the possible paths joining \mathbf{r}_0 and \mathbf{r}_1 by selecting the particular path that extremizes the circulation of the magnetic vector potential, yielding

$$d\mathbf{r} \times \mathbf{B} = 0, \tag{5}$$

which also derives from v = dr/dt and $B = \nabla \times A$ in Equation (3). Equivalently, the magnetic field lines are the instantaneous family of solutions of the ordinary differential equation (see, e.g., Longcope 2005)

$$\frac{d\mathbf{r}}{ds} = \mathbf{b}(\mathbf{r}),\tag{6}$$

where b(r) = B/B is the unit vector in the magnetic field direction and s is the arc length. We observe that, when evaluated along a magnetic field line, the integral in Equation (3) reads $\int_{r_0}^{r_1} A \cdot dr = \int_{s_0}^{s_1} (A \cdot B/B) ds$, an expression involving the magnetic helicity density $h_m = A \cdot B$. This line integral is the field line helicity (Antiochos 1987; Berger 1988). The field line helicity is ill-defined on stochastic magnetic field lines (Jokipii & Parker 1969) having infinite path length (Yeates & Hornig 2016). We will not dwell on the variational principles, which are, however, essential in constructing a Hamiltonian description of the magnetic field lines. Our main point here was to draw the connection between the magnetic field lines and the particle paths in the limit where the gyroradius is zero.

For a given $\mathbf{r}(s_0 = 0) = \mathbf{r}_0$, the ordinary differential Equation (6) is known to possess a unique solution, representing the magnetic field line that emanates from the location r_0 , only if the magnetic field nowhere vanishes and if it satisfies certain regularity conditions. Therefore, for a given model of the heliospheric magnetic field B(r), it is in principle possible to integrate Equation (6) in order to obtain the magnetic field lines $r(r_0, s)$ which are s-parameterized curves labeled by $r_0 = r(s = s_0)$. The ensemble of solutions of Equation (6) defines a deterministic field line mapping that is invertible. We notice that when the solution $r(s, s_0)$ is itself invertible, i.e., when $r(s, s_0)$ is not multivalued, one can in principle use the radial distance r instead of s in order to parameterize the magnetic field lines, which can thus be expressed as $[\theta(r), \phi(r)]$ in this case. Let us define a magnetic field line density distribution $f_m(\mathbf{r}, s)$ from the solution of the continuity equation

$$\frac{\partial f_m}{\partial s} + \nabla \cdot (\mathbf{b} f_m) = 0, \tag{7}$$

in such a way that the characteristics of this partial differential equation are the magnetic field lines. Equation (7) is a continuity equation for the density distribution f_m in three-dimensional space.

We observe that the guiding center trajectories of the particles, electrons, and ions, propagating at a constant speed v along the magnetic field lines, are governed by the equation

$$\frac{d\mathbf{r}}{dt} = \mu v \mathbf{b}(\mathbf{r}),\tag{8}$$

where μ is the pitch-angle cosine. Equation (8) for the guiding center trajectories derives from Equation (6) by using $s = \mu vt$. Therefore, it can be useful to think of the magnetic field lines as streams of scatter-free guiding centers moving at a constant speed and to think of s as time. It follows from Equation (8) that the guiding center trajectories are the characteristics of the equation

$$\frac{\partial f}{\partial t} + \nabla \cdot (\mu v \mathbf{b} f) = 0, \tag{9}$$

where $f(\mathbf{r}, t)$ is the three-dimensional particle density distribution and both μ and v are here considered to remain constant. Equation (9) is the common basis of more complex drift kinetic equations for the particle guiding centers. In Equation (9), only the effects of field-aligned streaming are retained. As a matter of fact, setting the pitch-angle cosine $\mu=1$ in a drift kinetic equation ought to nullify all the terms related to finite Larmor radius effects, only maintaining the field-aligned streaming term. A main tenet in this work is the equivalence between the magnetic field lines and the particle paths, under the restrictions invoked above: a vanishingly small gyroradius under scatter-free conditions.

We emphasize that on most scales of interest the field intensity B is nonuniform with a direction b that ought to be changing owing to the solenoidality condition for the magnetic field. It follows that the Jacobian determinant of the map $r_0 \rightarrow r^s(r_0)$ generated by Equation (6) is generally nonzero, and hence the map does not preserve volume on global scales. Equivalently said, the vector flow generated by nonuniform magnetic fields via Equation (6) is compressible. The degree of local compressibility of the flow can be characterized by the length scale L_b defined by

$$\frac{1}{L_B} = \left| \frac{\partial \ln B}{\partial s} \right| = \left| \nabla \cdot \boldsymbol{b} \right|. \tag{10}$$

The focusing/mirroring length L_b measures the local rate of exponentiation of the magnetic field strength per unit of the field-aligned distance. More generally, characterizing how the magnetic field lines behave locally can be done through the Jacobian matrix ∇b , the trace of which is L_B^{-1} . The Jacobian matrix enters the equation describing the separation vector between pairs of magnetic field lines, which reads $d\delta r/ds = \nabla b \cdot \delta r$. The local rate of exponentiation of the separation distance between pairs of magnetic field lines, per unit of field-aligned distance s, is the Lyapunov exponent, and it is defined as $L_L^{-1} = \partial \ln \delta r/\partial s$. Local exponential separation between pairs of solutions of ordinary differential equations such as Equation (6), as $\delta r_0 \rightarrow 0$, is the hallmark of the dynamical system sensitivity to the initial conditions: the

hallmark of chaos (Lorenz 1963). In turbulence, the rate of separation between pairs of magnetic field lines is faster than exponential, yielding stochastic instead of chaotic magnetic field lines (Eyink et al. 2011). The magnetic fields (and the velocity fields) are not differentiable functions of space in the infinite Reynolds number limit of the turbulence (Eyink et al. 2011).

The unperturbed magnetic field B(r), in the absence of solar wind turbulence, is the Parker (1958) field. In the heliographic coordinate system, a simple representation of the Parker field is given by

$$\boldsymbol{B}(r,\theta) = B_{0s} \left(\frac{r_0}{r}\right)^2 (\boldsymbol{u}_r - \tan \chi \boldsymbol{u}_\phi),$$

$$\cos \chi = \left[1 + \left(\frac{\Omega(r - r_0)\sin \theta}{V_{\text{sw}}}\right)^2\right]^{-1/2}, \quad (11)$$

where $V_{\rm sw}$ is the solar wind speed, Ω is the equatorial rotation rate of the Sun, and χ is the (winding) angle between the magnetic field and the radial direction. The Parker field is assumed to emanate from a source surface located at a distance $r = r_0$. It follows from Equation (11) that the magnetic field direction \boldsymbol{b} can be expressed in terms of χ as

$$\boldsymbol{b} = \cos \chi \boldsymbol{u}_r - \sin \chi \boldsymbol{u}_\phi. \tag{12}$$

The family of Parker spirals generates a simple invertible map between spatial points in the heliosphere. The magnetic connection between two spatial points in the heliosphere can be determined by selecting the curve that extremizes the circulation of the solar wind magnetic vector potential. It is not a too difficult task to obtain such a connection in absence of solar wind turbulence. Indeed, given the spacecraft location, denoted by r_{sp} , Equation (6), with b given by Equation (12), can be solved backward to the source surface $|r| = r_0$ in order to determine the angular location of the "source" at the Sun. Nevertheless, the magnetic field is turbulent, which significantly complicates the problem of determining the magnetic connection between the observer's location and the Sun. This difficulty was originally recognized by Jokipii & Parker (1969), who showed the importance of considering the statistical properties of the magnetic field lines in the solar wind. In the boundary-driven model by Jokipii & Parker (1969), the magnetic field fluctuations are produced by the turbulent motions of the magnetic footpoints on the photosphere, yielding a purely angular diffusion of the magnetic field lines. In this case, the angular density distribution $f_{ma}(\theta, \phi)$ $r \propto r^2 f_{\rm m}(\theta, \phi, r)$ of the magnetic field lines obeys the spherical drift diffusion equation (Bian & Li 2021)

$$\frac{\partial f_{\text{ma}}}{\partial r} - \frac{\Omega}{V_{\text{sw}}} \frac{\partial f_{\text{ma}}}{\partial \phi} = \frac{1}{\sin \theta} \frac{\partial}{\partial \theta} \sin \theta D_{\text{ma}}^{\text{JP}} \frac{\partial f_{\text{ma}}}{\partial \theta} + \frac{1}{\sin^2 \theta} \frac{\partial}{\partial \phi} D_{\text{ma}}^{\text{JP}} \frac{\partial f_{\text{ma}}}{\partial \phi}, \tag{13}$$

where $D_{\text{ma}}^{\text{JP}}$ is the angular diffusivity of the magnetic field lines. The latter is related to the angular diffusivity κ_a of the magnetic footpoints on the source surface by

$$D_{\rm ma}^{\rm JP} = \frac{\kappa_a}{V_{\rm var}}.$$
 (14)

It follows from Equation (13) that the boundary-driven stochastic Parker spirals are the solution of the stochastic differential equations (Bian & Li 2021)

$$\frac{d\theta}{dr} = \frac{D_{\text{ma}}^{\text{JP}}}{\tan \theta} + \sqrt{2D_{\text{ma}}^{\text{JP}}} \zeta_{\theta}(r),$$

$$\frac{d\phi}{dr} = -\left(\frac{\Omega}{V_{\text{sw}}}\right) + \frac{1}{\sin \theta} \sqrt{2D_{\text{ma}}^{\text{JP}}} \zeta_{\phi}(r).$$
(15)

The boundary-driven stochastic Parker spirals are sketched in Figure 7 of Jokipii & Parker (1969), and the solutions of Equation (15) are plotted in Figures 1 and 2 of Bian & Li (2021). We emphasize that the "random walk" of the magnetic field line is purely angular in all these figures. Stochastic Parker spirals are nowhere differentiable with infinite path lengths. Nevertheless, we can still use the arc length s along the unperturbed magnetic field in order to rewrite Equation (15) in the equivalent form (Bian & Li 2022a)

$$\frac{dr}{ds} = \cos \chi,
\frac{d\theta}{ds} = \frac{D_{\text{ma}}^{\text{JP}} \cos \chi}{\tan \theta} + \sqrt{2D_{\text{ma}}^{\text{JP}} \cos \chi} \zeta_{\theta}(s)
\frac{d\phi}{ds} = -\left(\frac{\Omega}{V_{\text{sw}}}\right) \cos \chi + \frac{1}{\sin \theta} \sqrt{2D_{\text{ma}}^{\text{JP}} \cos \chi} \zeta_{\phi}(s),$$
(16)

where we have used a well-known formula for deterministic and invertible "time changes" of stochastic processes. Moreover, using $s = \mu vt$ in Equation (16) yields the stochastic differential equation describing the ballistic transport of the particle guiding centers along the boundary-driven stochastic Parker spirals in the solar wind (Bian & Li 2022a). An important point to observe is that it is generally not appropriate to parameterize the heliospheric magnetic field line by r when r (s) becomes multivalued. It is the case when the solar wind magnetic fields switch back their direction toward the Sun (Dudok de Wit et al. 2020; Fargette et al. 2021). In situ turbulence in the solar wind is known to be mostly Alfvénic (Belcher & Davis 1971), here taken in the sense that it is dominated by Alfvén polarized fluctuations that are transverse to the guiding magnetic field (Schekochihin et al. 2009). This property is often referred to as variance or component anisotropy of the solar wind turbulence (Oughton et al. 2015). The guiding magnetic field is the Parker field whose direction becomes increasingly inclined with respect to the radial direction as the radial distance from the Sun increases; hence, transverse field fluctuations do possess a radial component in the solar wind. The presence of radial magnetic field fluctuations in the solar wind is not only expected from general considerations about the nature of the solar wind turbulence; it is also an observed property that has become the subject of renewed interest, in particular, in the context of magnetic switchbacks measured by the Parker Solar Probe (Dudok de Wit et al. 2020; Fargette et al. 2021).

A main objective in this work is to understand, from a statistical viewpoint, the role played by the radial component of the magnetic field fluctuations in the dispersion of the solar wind magnetic field lines and in the dispersion of energetic particles propagating scatter-free in the turbulent medium. It is more likely the case for electrons accelerated during solar flares (Lin 1974; Wang et al. 2011, 2016; Moradi & Li 2019). Qualitatively, it is expected to read as follows. Radial magnetic field fluctuations produce radial diffusion of the magnetic field lines, vielding a radial spread of the field line density distributions and hence also a radial spread of the guiding center density distributions, even when the particles propagate unscattered with $\mu = 1$ along the dispersing magnetic field lines. Via numerical simulations of the equation describing the evolution of the three-dimensional magnetic field line density distribution, we quantify these effects for a given model of the radial evolution of the solar wind turbulence. They are chiefly determined by the magnetic field line diffusivity and by geometrical factors associated with the configuration of the Parker field.

2.1. The Local Magnetic Field Line Diffusivity

The local dispersion of the magnetic field lines due to solar wind turbulence can be characterized by a magnetic field line diffusivity D_m estimated locally from measurements of the magnetic field fluctuations δB_r , δB_θ , and δB_ϕ at the spacecraft position. Solar wind turbulence can be considered locally homogeneous and stationary. Therefore, let us adopt a local Cartesian coordinate system at the spacecraft position, whose unit vector z coincides with the direction b of the Parker field as

$$z = b,$$

$$y = b \times x,$$

$$x = u_{\theta},$$
(17)

where u_{θ} is the latitudinal direction. In this local coordinate system, the turbulent magnetic field can be decomposed according to

$$\boldsymbol{B} = B_0 \boldsymbol{z} + \delta \boldsymbol{B}_1, \tag{18}$$

where the turbulent magnetic fluctuations $\delta {\pmb B}_\perp$ are transverse to ${\pmb z}$. We neglected the small contribution of $\delta {\pmb B}_z \ll \delta {\pmb B}_\perp$. It follows from the decomposition in Equation (18) that locally the magnetic field lines are the solutions of the ordinary differential equations

$$\frac{dz(s)}{ds} = \frac{B_0}{B},
\frac{d\mathbf{r}_{\perp}(s)}{ds} = \frac{\delta \mathbf{B}_{\perp}(\mathbf{r}_{\perp}, z)}{B}, \tag{19}$$

where $r_{\perp} = (x, y)$. Now eliminating s in this system results in the field line equation in the form

$$\frac{d\mathbf{r}_{\perp}(z)}{dz} = \frac{\delta \mathbf{B}_{\perp}(\mathbf{r}_{\perp}, z)}{B_0}.$$
 (20)

Equation (20) can be restated in terms of the *z*-component of the fluctuating vector potential, explicitly showing its Hamiltonian structure (Morrison 2000; Bian et al. 2011). Given that in the local frame the magnetic field lines $\mathbf{r}_{\perp}(z)$ do not cross twice the same plane perpendicular to the direction z, it is thus possible to define the magnetic field fluctuations evaluated along the magnetic field

lines as $\delta \pmb{B}_{\perp}(z) = \int \!\! \delta \pmb{B}_{\perp}(\pmb{r}_{\perp}, z) \delta(\pmb{r}_{\perp} - \pmb{r}_{\perp}(z)) d\pmb{r}_{\perp}$, where $\pmb{r}_{\perp}(z)$ satisfies Equation (20). Let us Fourier decompose the latter according to $\delta \pmb{B}_{\perp}(z) = \int e^{-ik_{\parallel}z} \delta \pmb{B}_{\perp}(k_{\parallel}) dk_{\parallel}$ and define the parallel wavenumber spectrum $E_B(k_{\parallel})$ as

$$E_{B}(k_{\parallel}) = \frac{1}{2\pi} \int e^{ik_{\parallel}\Delta z} \langle \delta \mathbf{B}_{\perp}(z + \Delta z) \cdot \delta \mathbf{B}_{\perp}(z) \rangle d\Delta z, \qquad (21)$$

an expression that involves the trace of the autocorrelation tensor. We emphasize that $E_B(k_{\parallel})$ is the spectrum of the magnetic field fluctuations evaluated along the magnetic field lines. It is different from $E_B(k_z)$, the spectrum of the magnetic field fluctuations evaluated along the direction z of the guiding magnetic field. In the solar wind, the spectrum $E_B(k_{\parallel})$ given by Equation (21) is measured to behave as a power law $k_{\parallel}^{-\alpha}$ with α close to 2 in the inertial range (Horbury et al. 2008; Podesta 2009; Wicks et al. 2010). The spectral index $\alpha = 2$ is predicted by theories elucidating the importance of the critical balance condition in Alfvénic turbulence (Goldreich & Sridhar 1995; Boldyrev 2006). Using Equation (6), it can be shown that (Jokipii & Parker 1969)

$$D_{m} \equiv \frac{1}{2} \frac{d \langle x^{2}(z) \rangle}{dz} = \frac{1}{B_{0}^{2}} \int_{0}^{\infty} \langle \delta B_{x}(0) \delta B_{x}(\Delta z) \rangle d\Delta z, \quad (22)$$

which is, by definition, the expression for the magnetic field line diffusivity D_m . Therefore, the magnetic field line diffusivity D_m can be expressed in terms of the parallel wavenumber spectrum as (Bian & Li 2022b)

$$D_m = \frac{\pi}{2} \frac{E_B(k_{\parallel} = 0)}{B_0^2},\tag{23}$$

involving the value of the spectral energy density $E_B(k_{\parallel})$ at $k_{\parallel} = 0$. Local axisymmetry of the magnetic field fluctuations in the plane perpendicular to z is implicitly assumed here. It follows that D_m can equivalently be defined in terms of the trace of the autocorellation tensor appearing in Equation (21), hence the factor of one-half difference between Equation (23) and the definition of D_m previously adopted in Bian & Li (2022b). The magnetic field line diffusivity is a function of space, and its radial dependence can in principle be obtained directly by spacecraft measurements of D_m made at various distances from the Sun. However, extraction of the spectrum $E_R(k_{\parallel})$ from the time series of magnetic field fluctuations recorded by spacecraft in the solar wind requires a complex wavelet analysis of the data set (Horbury et al. 2008; Podesta 2009; Wicks et al. 2010). Given the apparent difficulty in measuring the spectrum $E_B(k_{\parallel})$ and in extrapolating it to $k_{\parallel} = 0$, it has become standard to estimate the field line diffusivity D_m from the spectrum $E_B(k_z, k_\perp)$, which is easier to measure. Certain model assumptions are, however, needed in this case in order to functionally relate $E_B(k_z, k_\perp)$ to the value $E_B(k_{\parallel}=0)$, which ultimately determines the magnetic field line diffusivity D_m . These model assumptions are almost invariably based on the Corrsin (1959) hypothesis introduced by Matthaeus et al. (1995) in the context of magnetic field line diffusion. The Corrsin (1959) hypothesis relates Eulerian and Lagrangian statistics (Bian & Li 2022b): it relates the statistical properties of the magnetic field fluctuations in the Eulerian frame to those of the magnetic field fluctuations evaluated along the magnetic field lines.

On local scales, the dispersion of magnetic field lines can be described by the diffusion equation (Chandrasekhar 1943; Jokipii & Parker 1969),

$$\frac{\partial f_m}{\partial \tau} = \nabla_{\perp} \cdot (D_m \nabla_{\perp} f_m), \tag{24}$$

where $f_m(\mathbf{r}_{\perp}, z)$ represents the local magnetic field line distribution function, D_m is the scalar constant given in Equation (23), and ∇_{\perp} is the transverse component of the ∇ -operator in the slab. The solution of Equation (24) including a source term in the form of $\delta(\mathbf{r}_{\perp})\delta(z)$ on the right-hand side is the two-dimensional Gaussian distribution. We can define the average magnetic field line from the first moment of the magnetic field line distribution function f_m , which is the solution of Equation (24), as

$$\langle \mathbf{r}_{\perp}(z) \rangle = \frac{\int \mathbf{r}_{\perp} f_m d\mathbf{r}_{\perp}}{\int f_m d\mathbf{r}_{\perp}}.$$
 (25)

Multiplying Equation (24) by r_{\perp} and taking on both sides the integral over the perpendicular spatial coordinates yields

$$\frac{d\langle \mathbf{r}_{\perp}(z)\rangle}{dz} = 0, \tag{26}$$

after two integrations by parts. This proves that the average magnetic field line does not drift from the direction z along the guiding magnetic field. We note that each individual magnetic field line emanating from the point source can be represented by the realization of a two-dimensional Wiener process $\mathbf{r}_{\perp}^{i}(z) = \sqrt{2D_{m} \mathbf{W}^{i}(z)}$, where the superscript i labels a given realization. The sum $\sum_{i=1}^{N} r_{\perp}^{i}(z)/N$ is a function of z converging pointwise to 0 when $N \rightarrow \infty$, which is another way of showing that $\langle \mathbf{r}_{\perp}(z) \rangle = 0$. Since the process underlying Equation (24) is Gaussian, magnetic field line dispersion is uniquely characterized by the second-order moment of the magnetic field line distribution function, which obeys $\langle r_{\perp}^{2}(z)\rangle = 4D_{m}z$. These well-known properties of the isotropic diffusion process with a spatially constant diffusivity do not generalize to the inhomogeneous case (Cherstvy et al. 2013) that will be considered below. Before this, let us again discuss the equivalence between the spatial dispersion of particles in stochastic magnetic fields, in the limit of a zero gyroradius, and that of the magnetic field lines. Jokipii (1966) and Jokipii & Parker (1969) established that the guiding center density distribution satisfies the kinetic equation

$$\frac{\partial f}{\partial t} + \frac{\partial}{\partial z}(\mu \nu f) = \frac{\partial}{\partial \mu} \left(D_{\mu\mu} \frac{\partial f}{\partial \mu} \right) + \nabla_{\!\perp} \cdot (D \nabla_{\!\perp} f), \qquad (27)$$

where D is the perpendicular spatial diffusivity of the particles and $D_{\mu\mu}$ is the pitch-angle diffusivity resulting from turbulent scattering. The guiding magnetic field is taken to be uniform and directed along z, and thus there is no need to consider the mirroring/focusing effect resulting from the conservation of the first adiabatic invariant (Roelof 1969; Earl 1976; Litvinenko 2012). Equation (27) is the same as Equation (31) in Jokipii & Parker (1969). Jokipii (1966) has shown that the perpendicular

diffusivity D can be split into two contributions arising from the spatial diffusion of the magnetic field lines and from the resonant scattering of the particles. The resonant scattering contribution to D is a finite Larmor radius effect, as is $D_{\mu\mu}$, which vanishes for $\mu=1$. Taking $\mu=1$ in Equation (27) yields

$$\frac{\partial f}{\partial t} + \frac{\partial}{\partial z}(vf) = \nabla_{\perp} \cdot (D\nabla_{\perp} f). \tag{28}$$

Dividing Equation (28) by the constant speed v, introducing the traveled length s = vt along the guiding magnetic field, and identifying the particle density distribution function f with the magnetic field line distribution function f_m results in the three-dimensional convection–diffusion equation

$$\frac{\partial f_m}{\partial s} + \frac{\partial f_m}{\partial z} = \nabla_{\perp} \cdot (D_m \nabla_{\perp} f_m), \qquad D_m = \frac{D(\mu = 1)}{v}, \quad (29)$$

which provides essentially the same information as the twodimensional diffusion Equation (24). We emphasize, however, that f_m is a three-dimensional density distribution (cm⁽⁻⁾³) in Equation (29). It is given by

$$f_m(x, y, z, s) = \frac{\delta(z - s)}{4\pi D_m s} e^{-\frac{(x^2 + y^2)}{4D_m s}}.$$
 (30)

Substituting s = vt in the right-hand side of Equation (30) yields the particular solution $f(x, y, z, \mu = 1, t)$ of Equation (27) obtained by setting $D_{\mu\mu} = 0$. It describes the time evolution of the three-dimensional density distribution function of scatterfree particles after being released with $\mu = 1$ at the origin of this Cartesian coordinate system. We note that all the particles cross the plane z = cst at the same time despite the perpendicular dispersion. This is not an important issue when it comes to the modeling of the spatial spread, but it is one that needs to be taken into consideration in order to accurately model the effect of cross-field diffusion on the arrival times of the particles. The apparent paradox boils down to the fractal structure of the Brownian magnetic field lines having no definite length. It follows from the Fokker-Planck Equation (29) that the realizations of the stochastic magnetic field lines are obtained by solving the stochastic differential equations

$$\frac{dz}{ds} = 1$$

$$\frac{dx}{ds} = \sqrt{2D_m} \zeta_x(s)$$

$$\frac{dy}{ds} = \sqrt{2D_m} \zeta_y(s),$$
(31)

where $\zeta_x(s)$ and $\zeta_y(s)$ are unit Gaussian white noises. The solutions of Equation (31) are represented by the two-dimensional Wiener process

$$\mathbf{r}_{\perp}(z) = \sqrt{2D_m} \mathbf{W}(z). \tag{32}$$

The stochastic magnetic field lines have been "extracted" from a model of stochastic particle motions by taking the limit of a vanishingly small gyroradius, i.e., by taking $\mu = 1$ in the kinetic equation describing the particle motions as a function of time. We used here the kinetic equation established by Jokipii (1966) and Jokipii & Parker (1969) in a local slab. The

very same procedure can be generalized and applied to global heliospheric scale transport models.

2.2. Global Magnetic Field Line Dispersion in the Heliosphere

Our starting point is the global scale generalization of Equation (27) studied by Strauss & Fichtner (2015), Strauss et al. (2017), and Strauss & le Roux (2019). It reads

$$\frac{\partial f}{\partial t} + \nabla \cdot (\mu \nu \boldsymbol{b} f) + \frac{\partial}{\partial \mu} \left[\frac{(1 - \mu^2)}{L_B} \nu f \right]
= \frac{\partial}{\partial \mu} \left(D_{\mu\mu} \frac{\partial f}{\partial \mu} \right) + \nabla \cdot (\boldsymbol{D} \cdot \nabla f), \tag{33}$$

where D is the guiding center diffusivity tensor, b(r) is the direction of the background magnetic field given here by Equation (12), and L_B is the focusing length given by Equation (10). Setting $\mu=1$ cancels all the finite Larmor radius effects in Equation (33), leaving us with an equation for the magnetic field lines. Therefore, the diffusion of stochastic Parker spirals on global heliospheric scales in the solar wind can be described by the convection–diffusion equation

$$\frac{\partial f_m}{\partial s} + \nabla \cdot (\boldsymbol{b} f_m) = \nabla \cdot (\boldsymbol{D}_m \cdot \nabla f_m), \tag{34}$$

where $f_m(\mathbf{r}, s)$ is the heliospheric magnetic field line distribution function and $D_m(\mathbf{r})$ is the field line diffusion tensor. Let us first observe that Equation (34) with $D_m = 0$ reduces to Equation (7), whose characteristics are the Parker spirals. Therefore, s can be interpreted as the arc length along the Parker field. A physical interpretation of s is not mandatory in order to obtain the solutions of the convection-diffusion Equation (34). Its nature need not even be specified provided that it parameterizes the magnetic field lines. More importantly, we observe that because both b and D_m are functions of r, the solutions of the convection-diffusion Equation (34) are generally not Gaussian distributions. Multiplying Equation (34) by r and carrying an integration over space yields

$$\frac{d\langle \boldsymbol{r}(s)\rangle}{ds} = \int [f_m(\nabla \cdot \boldsymbol{D}_m + \boldsymbol{b})]d\boldsymbol{r}, \tag{35}$$

which should be compared with Equation (26). In Equation (35), $\nabla \cdot \mathbf{D}_m$ plays a role similar to \mathbf{b} , showing that the direction of the average magnetic field line $\langle \mathbf{r}(s) \rangle$ may *not* generally coincide with the direction \mathbf{b} of the background magnetic field.

It remains to relate the form of the diffusion tensor D_m entering Equation (34) to the local magnetic field line diffusivity D_m . In the global heliographic coordinate system, the diffusion tensor D_m in Equation (34) takes the form of a 3×3 matrix that is generally not diagonal. The nine components of D_m in the heliographic coordinate system can be obtained by noticing that in the local Cartesian frame given by Equation (17) the diffusion tensor is diagonal and given by

$$\boldsymbol{D}_{m}^{L} = \begin{pmatrix} 0 & 0 & 0 \\ 0 & D_{m} & 0 \\ 0 & 0 & D_{m} \end{pmatrix} \tag{36}$$

for Alfvénic magnetic field fluctuations transverse to z. Therefore, the form of the field line diffusion tensor D_m entering Equation (34), expressed in the heliographic coordinate system, can be obtained from D_m^L in Equation (36) by applying the transformation

$$\boldsymbol{D}_{m} = \boldsymbol{R} \boldsymbol{D}_{m}^{L} \boldsymbol{R}^{T}, \tag{37}$$

where the superscript T denotes the transpose operation and R represents the Parker angle rotation,

$$\mathbf{R} = \begin{pmatrix} \cos \chi & 0 & \sin \chi \\ 0 & 1 & 0 \\ -\sin \chi & 0 & \cos \chi \end{pmatrix}. \tag{38}$$

This yields

$$\boldsymbol{D}_{m} = \begin{pmatrix} D_{m}^{rr} = D_{m} \sin^{2} \chi & D_{m}^{r\theta} = 0 & D_{m}^{r\phi} = D_{m} \sin \chi \cos \chi \\ D_{m}^{\theta r} = 0 & D_{m}^{\theta \theta} = D_{m} & D_{m}^{\theta \phi} = 0 \\ D_{m}^{\phi r} = D_{m} \sin \chi \cos \chi & D_{m}^{\phi \theta} = 0 & D_{m}^{\phi \phi} = D_{m} \cos^{2} \chi \end{pmatrix}.$$

$$(39)$$

It follows from expressing the convection–diffusion Equation (34) in the heliographic coordinate system that the heliospheric magnetic field line density distribution f_m obeys the equation

$$\frac{\partial f_m}{\partial s} + \frac{1}{r^2} \frac{\partial r^2 \cos \chi f_m}{\partial r} - \frac{1}{r \sin \theta} \frac{\partial \sin \chi f_m}{\partial \phi} \\
= \frac{1}{r^2} \frac{\partial}{\partial r} r^2 D_m^{rr} \frac{\partial f_m}{\partial r} + \frac{1}{r \sin \theta} \frac{\partial}{\partial \phi} D_m^{\phi r} \frac{\partial f_m}{\partial r} \\
+ \frac{1}{r^2 \sin \theta} \frac{\partial}{\partial \theta} \sin \theta D_m^{\theta \theta} \frac{\partial f_m}{\partial \theta} \\
+ \frac{1}{r^2 \sin^2 \theta} \frac{\partial}{\partial \phi} D_m^{\phi \phi} \frac{\partial f_m}{\partial \phi} + \frac{1}{r^2 \sin \theta} \frac{\partial}{\partial r} r D_m^{r\phi} \frac{\partial f_m}{\partial \phi}, \tag{40}$$

where the various components D_m^{ij} , with $i,j=r,\theta,\phi$, are given in Equation (39). Equation (40) constitutes the general model describing the diffusion of magnetic field lines on global heliospheric scales in the case where the background magnetic field is the Parker field. We observe from the expression for the diffusion tensor \boldsymbol{D}_m given by Equation (39) the existence of a purely radial component and the presence of nondiagonal drift components. The radial component $D_m^{rr} \sim D_m \chi^2$ and the nondiagonal components $D_m^{\phi r} = D_m^{r\phi} \sim D_m \chi$ close to the Sun where $\chi \ll 1$.

The convection–diffusion Equation (40) can be reformulated as a Fokker–Planck equation for the magnetic field line probability distribution function $P(\mathbf{r}, s) = r^2 \sin \theta f_{\rm m}(\mathbf{r}, s)$, and hence the magnetic field lines $\mathbf{r}(s)$ are the solutions of a set of stochastic differential equations. The differential equations for the stochastic Parker spirals are cumbersome, and thus they will not be written down here. Nevertheless, the two approaches based on the Fokker–Planck equation, which is a partial differential equation for $P(\mathbf{r}, s)$, and based on the differential equation for its stochastic characteristics $\mathbf{r}(s)$ are equivalent. The present field line mapping model differs from the ballistic field line mapping models adopted in the past (Schatten et al. 1968; Nolte & Roelof 1973; Li et al. 2016) in that the deviations from the Parker field, or from any other fields chosen to be the background (Fisk 1996, 2001; Burger et al. 2008) in our

model, are due to statistical effects resulting from solar wind turbulence combined with those of the background field geometry.

3. Numerical Solutions

Equation (40) is solved numerically in the equatorial plane corresponding to $\theta = \pi/2$, where it reduces to

$$\frac{\partial f_m}{\partial s} + \frac{1}{r^2} \frac{\partial r^2 \cos \chi f_m}{\partial r} - \frac{1}{r} \frac{\partial \sin \chi f_m}{\partial \phi} \\
= \frac{1}{r^2} \frac{\partial}{\partial r} r^2 D_m^{rr} \frac{\partial f_m}{\partial r} + \frac{1}{r} \frac{\partial}{\partial \phi} D_m^{\phi r} \frac{\partial f_m}{\partial r} \\
+ \frac{1}{r^2} \frac{\partial}{\partial \phi} D_m^{\phi \phi} \frac{\partial f_m}{\partial \phi} + \frac{1}{r^2} \frac{\partial}{\partial r} r D_m^{r\phi} \frac{\partial f_m}{\partial \phi}.$$
(41)

For the simulations shown in this section we assume, as a first approach, generic solar minimum values of the various plasma quantities relevant to this study. This is motivated by the fact that both large-scale plasma quantities such as the solar wind and helisopheric magnetic field (see, e.g., Owens & Forsyth 2013) and small-scale turbulence quantities such as magnetic variances (see, e.g., Zhao et al. 2018; Burger et al. 2022) vary considerably less during periods of lower solar activity. Therefore, we adopt a Parker field produced by a solar wind speed of 400 km s⁻¹. The radial dependence of the magnetic field line diffusivity $D_m(r)$ is calculated using the approach outlined by Strauss et al. (2017), where a theoretically (Matthaeus et al. 2007) and observationally motivated piecewise continuous two-dimensional spectrum $E_B(k_{\perp})$ is used and scaled with turbulence observations corresponding to solar minimum conditions, including the radial dependence of the magnetic field fluctuation variance $\langle \delta B_{\perp}^{2}(r) \rangle$. The method is based on the earlier approach of Engelbrecht & Burger (2015). Note that although the turbulence parameters that D_m depends on are known to be solar cycle dependent, this dependence may not be so significant owing to the fact that D_m is a function of the ratio of the magnetic variance to the background magnetic field magnitude. Therefore, such a solar cycle dependence would have to come from the weaker solar cycle dependence seen in the magnetic correlation scale (e.g., Engelbrecht & Wolmarans 2020) and may not significantly influence the results presented here. At the inner boundary $r_0 = 0.05$ au, the following condition is specified:

$$f_m(r = r_0, \phi, s) = C \exp\left[-\frac{(\phi - \phi_0)}{2\sigma^2}\right] g(s),$$
 (42)

representing a Gaussian longitudinal source with narrow broadness $\sigma=5^\circ$ centered at $\phi_0=90^\circ$ at the Sun. The function g(s) is taken either as a delta-function $g(s)=\delta(s)$ or as a constant g(s)=1. The constant C is a normalization factor. At the outer boundary $r_{\rm out}=10\,{\rm au}$, the absorbing boundary condition

$$f_{\rm m}(r = r_{\rm out}, \, \phi, \, s) = 0$$
 (43)

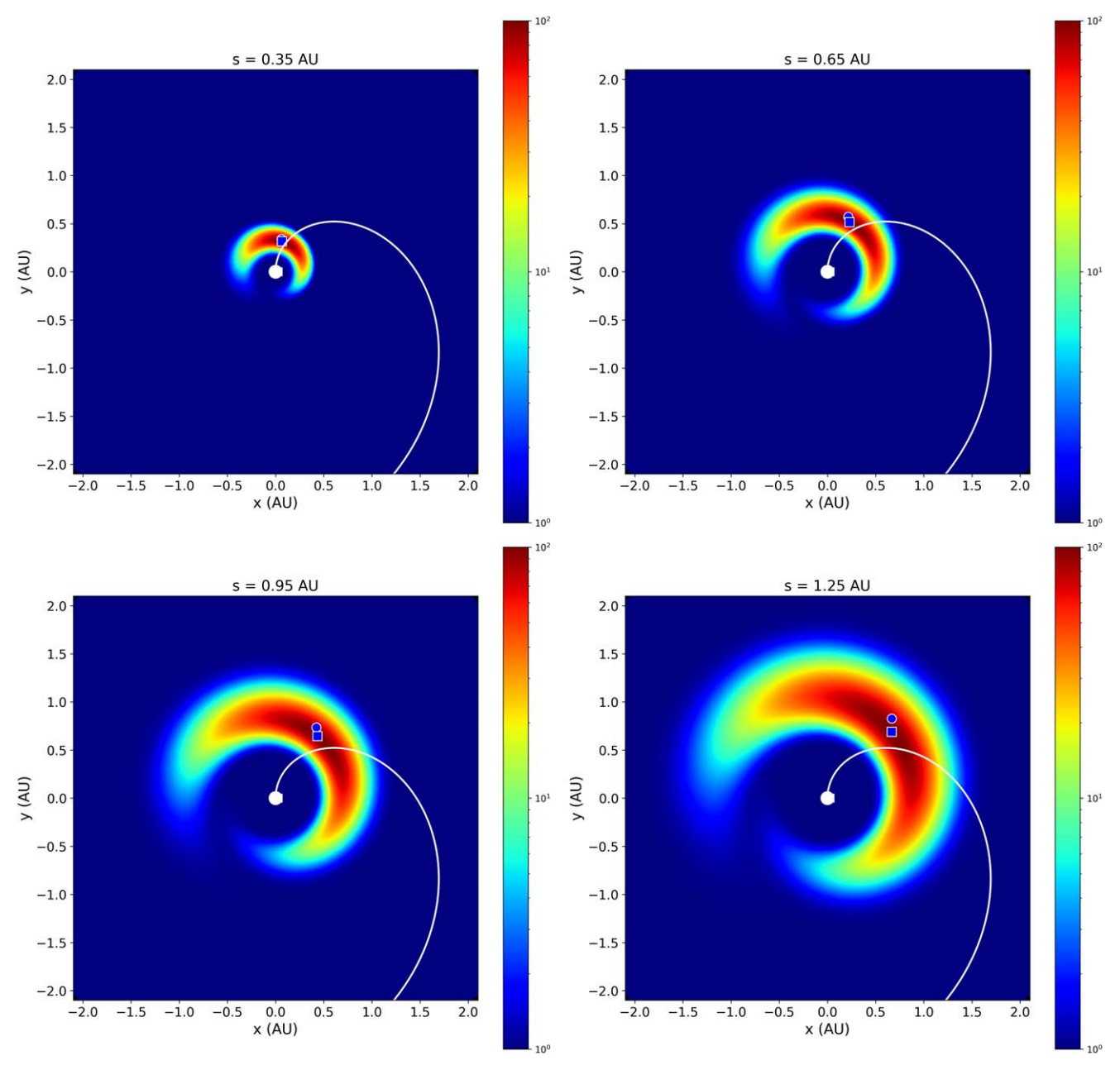


Figure 1. Diffusion of stochastic Parker spirals in the solar wind. The contour plot represents the magnetic field line distribution function in the equatorial plane for increasing values of s in astronomical units. The nominal Parker spiral emanating at $\phi = 90^{\circ}$ is represented by the white curve. The squares and circles correspond to the most probable and the mean values of the field line distribution, respectively.

is specified. It follows that the magnetic field lines or the particles escaping the outer boundary cannot reenter the simulation domain.

Let us first consider the solution $f(\mathbf{r}, s)$ of Equation (41) in the case where $g(s) = \delta(s)$. We define the moment

$$\langle \boldsymbol{r}(s) \rangle = \frac{\iint r f_m r^2 dr d\phi}{\iint f_m r^2 dr d\phi}.$$
 (44)

For a given s, $\langle r(s) \rangle$ represents the mean value of the field line distribution. Therefore, the function $\langle r(s) \rangle$ also represents the average magnetic field line emanating from the source at the Sun. We recall that, in the stochastic differential equation formulation of the same diffusion problem, the average field

line can equivalently be defined as $\langle r(s) \rangle = \sum_{i=1}^N r^i(s)/N$, where $r^i(s)$ are $N \to \infty$ realizations of the stochastic process representing the magnetic field lines emanating from the same source at the Sun. Figure 1 displays the magnetic field line distribution function $f_m(r, \phi, s)$ for increasing values of s. The nominal Parker spiral emanating from the source located at $\phi = 90^\circ$ at the Sun is represented by the white curve. We observe that as s increases the magnetic field line distribution becomes broader in longitude. The magnetic field line distribution becomes also radially broader. The longitudinal broadening and radial broadening of the distribution are due to the longitudinal and radial components of the diffusion process. They enter as the diagonal components of D_m in Equation (39). Radial broadening of the distribution is substantial although

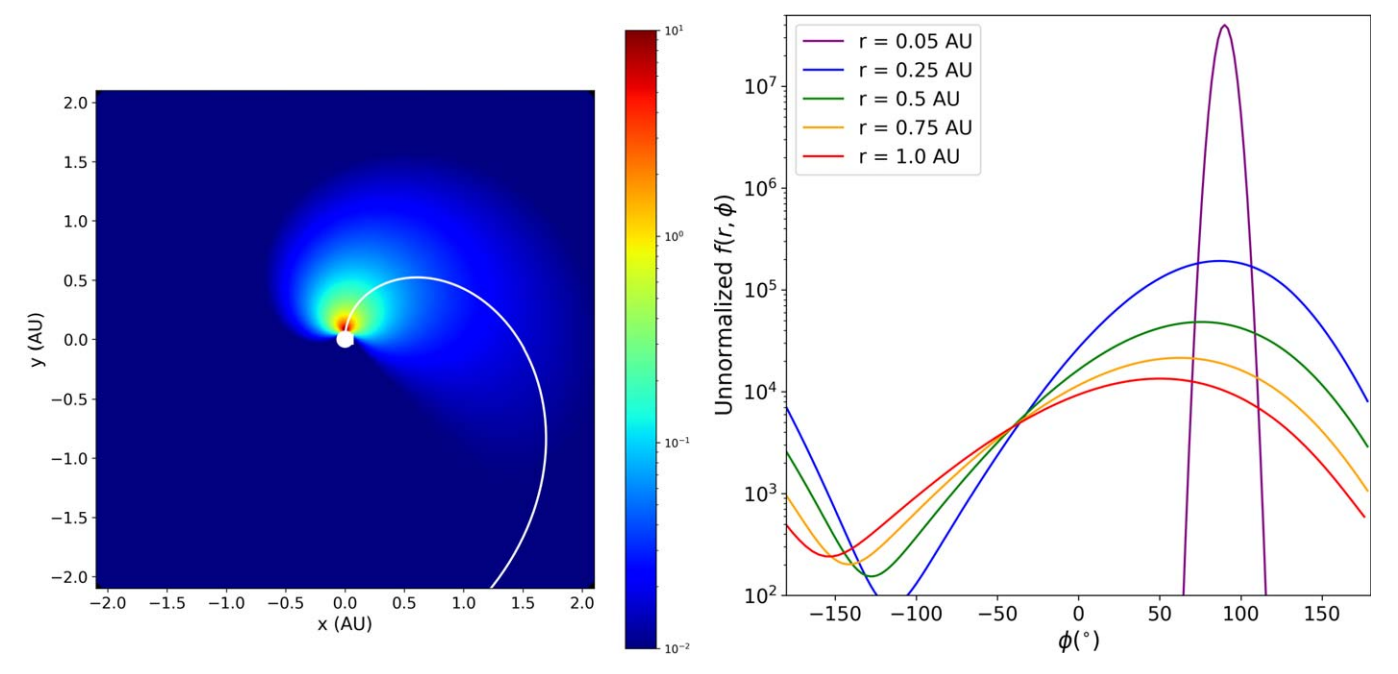


Figure 2. The left panel shows the simulated steady-state solution of f_m as a contour plot in the equatorial plane of the heliosphere. A nominal Parker magnetic field line is again shown as the solid white line. The right panel shows the field line angular distributions at various radial distances r, corresponding to the results displayed in the left panel.

less pronounced than longitudinal broadening. There is also a noticeable shift of the distribution counterclockwise. This shift is due to the effects of the drift terms corresponding to the nondiagonal components of the field line diffusion tensor in Equation (39). The squares and circles in Figure 1 correspond to the most probable and mean values of the field line distribution, respectively. They are both shifted with respect to the Parker field line. Therefore, the results show that the mean $\langle r(s) \rangle$ is different from the Parker spiral, which is obtained by solving the same equation with the field line diffusivity set to zero, i.e., it is different from the solution of the purely deterministic component of its characteristic equation given by Equation (6), with b given by Equation (12). The observed phenomenon is due to the spatial inhomogeneity of the diffusion tensor D_m . The phenomenon can be pinpointed through the $\nabla \cdot \mathbf{D}_m$ term in Equation (35) governing the firstorder moment. The distributions displayed in Figure 1 can be interpreted as the spatial distributions of particle guiding centers, electrons and ions, promptly injected with a pitchangle cosine $\mu = 1$ from the solar source and propagating scatter-free outward at a constant speed v along the diffusing magnetic field lines. In this interpretation, time is measured in units of the traveled distance according to

$$t = \frac{s}{v},\tag{45}$$

where the speed v of the injected particles is constant. Despite the absence of pitch-angle scattering, the radial broadening of the particle distribution function appears similar to that of pitch-angle scattering. It follows that due to the radial diffusion of the magnetic field lines, we expect a dispersion in the crossing times of the particles at a distance r from the source similar to, but nevertheless distinct from, the delay-time distribution resulting from pitch-angle scattering

(Bian & Emslie 2019, 2020). Radial diffusion of the magnetic field lines thus constitutes an additional source of interpretations of the results obtained from velocity dispersion analysis applied to the onset time of SEP events (Lin 1974; Krucker & Lin 2000; Tylka et al. 2003; Sáiz et al. 2005; Wang et al. 2016; Zhao et al. 2019), which is based on Equation (45).

We now repeat the calculations with g(s) = 1. The numerical code is run until the solution f_m of Equation (41) becomes independent of s. The result is shown in the left panel of Figure 2 as a contour plot of the distribution f_m . The longitudinal distributions at different radial distances are shown in the right panel. The distribution shown in the left panel can be interpreted as the spatial distribution of scatterfree particles steadily injected with $\mu = 1$ at the solar source and steadily removed at the outer boundary. The angular distributions in the right panel of Figure 2 can thus be interpreted as steady-state longitudinal distributions of scatterfree particles at various values of r. We also compute the mean and variance of the longitudinal distributions. Their dependence on r is plotted in the left panel of Figure 3. Also shown is the longitudinal position of the nominal Parker magnetic spiral (blue dashed line). The right panel of the figure shows the nominal Parker spiral (solid line) compared to the curve given by the longitudinal mean value (dashed line) as a function of r. They both represent Archimidean spirals. However, it is clearly apparent that the average magnetic field line computed from the obtained distribution is underwound with respect to the unperturbed Parker field line. The spiral angle at Earth's orbit obtained from the model is 43° at 1 au compared to 47° for the Parker spiral at the same solar wind speed. For an observer looking at the Sun, the position of the most probable connecting magnetic field line on the solar disk, after accounting for solar wind turbulence, is shifted by about 10° westward with respect to prediction of the Parker (1958) model. After accounting for solar wind turbulence in the model, the Archimedean spiral best connecting the observer to the Sun

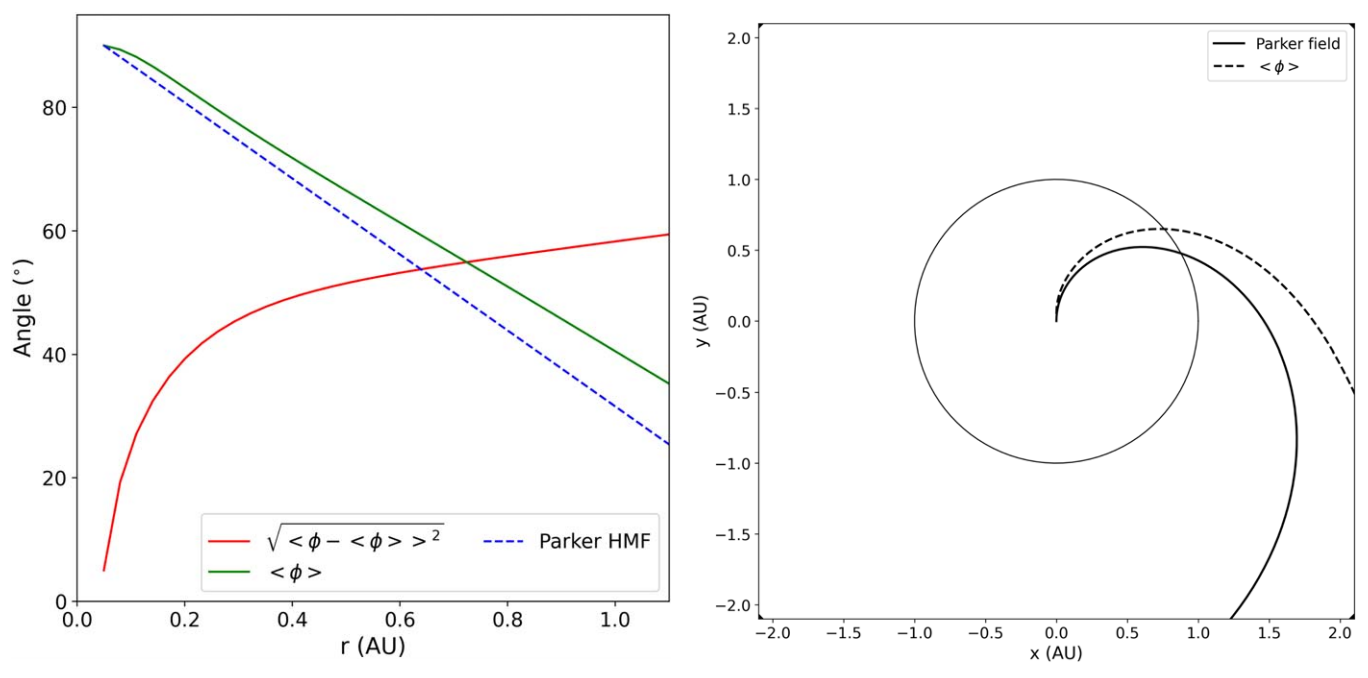


Figure 3. Left: mean (green line) and variance (red line) of the simulated angular field line distribution as a function of radial distance using the results of Figure 2. The nominal Parker spiral (blue dashed line) is also shown. Right: the nominal Parker spiral (solid line) and the mean value of the magnetic field distribution from the simulations (dashed line) shown in the equatorial plane. The circle shows Earth's orbit for reference.

is shorter than the Parker spiral. The length of the Parker spiral is 1.21 au at 1 au for a solar wind speed of 400 km s⁻¹. In our model, the best connecting magnetic field line is more radial. It has a length of 1.14 au at 1 au, a value that is about 5% shorter than in the Parker model.

4. Longitudinal Diffusion

Let us make the ansatz that the longitudinal distribution of magnetic field lines around its mean value obeys the circular diffusion equation

$$\frac{\partial f_{\text{ma}}}{\partial r} = \frac{\partial}{\partial \Delta \phi} D_{\text{ma}}(r) \frac{\partial f_{\text{ma}}}{\partial \Delta \phi},\tag{46}$$

where the coefficient $D_{\rm ma}(r)$ represents the field line longitudinal diffusivity that is related to the component $D_m^{\phi\phi}(r)$ by

$$D_{\rm ma}(r) = \frac{D_m^{\phi\phi}(r)}{r^2}.\tag{47}$$

Applying the method of images, the solution of Equation (46) can be expressed as a wrapped Gaussian distribution (Bian & Li 2022a) given by

$$f_{\text{ma}}(\Delta\phi, r) = \frac{1}{\sqrt{2\pi\sigma^2(r)}} \sum_{n=-\infty}^{+\infty} \exp\left[-\frac{(\Delta\phi + 2\pi n)^2}{2\sigma^2(r)}\right],$$
(48)

where $\Delta \phi = \phi - \langle \phi(r) \rangle$ is the deviation from the mean $\langle \phi(r) \rangle$. The circular distribution in Equation (48) is an infinite sum of Gaussian distributions, all having a common variance given by

$$\sigma^{2}(r) = \sigma^{2}(r_{0}) + 2 \int_{r_{0}}^{r} D_{\text{ma}}(r') dr'.$$
 (49)

At small enough longitudinal spread, the distribution $f_{\rm ma}(\Delta\phi, r)$ in Equation (48) can be approximated by its n = 0 component in the sum. Equation (49) predicts the radial evolution of the longitudinal variance of the angular distribution. We computed the radial derivative of the numerically obtained longitudinal variance $\sigma^2(r)$, i.e., the radial derivative of the red curve in the left panel of Figure 3. The result is plotted in Figure 4 and compared with twice the angular diffusivity $D_{\text{ma}}(r) = D_m(r)/r^2$, which is used as input in the numerical simulations. These two quantities are shown to compare relatively well for not too large angular spreads, where the Gaussian approximation to the circular Gaussian remains valid. The large angle saturation of the variance is a geometrical effect: it is a natural consequence of the periodic geometry that is accounted for by the circular Gaussian model but not by the Gaussian model. The wrapped Gaussian model cannot, however, account for the western skewness, which, albeit not being too pronounced, is nevertheless appreciable in the angular distributions displayed in the right panel of Figure 2. A more accurate fit of the angular distributions could in principle be obtained by wrapping a skew-Gaussian distribution around the circle.

5. Discussions and Conclusion

In their seminal works, Jokipii (1966) and Jokipii & Parker (1969) established the drift kinetic equation for the time evolution of the three-dimensional guiding center density distribution function $f(\mathbf{r}, \mu, t)$,

$$\frac{\partial f}{\partial t} + \frac{\partial}{\partial z}(\mu \nu f) = \frac{\partial}{\partial \mu} \left(D_{\mu\mu} \frac{\partial f}{\partial \mu} \right) + \nabla_{\!\perp} \cdot (D \nabla_{\!\perp} f), \quad (50)$$

where μ is the pitch-angle cosine and v the constant particle speed. The two scalar coefficients $D_{\mu\mu}$ and D are the pitch-

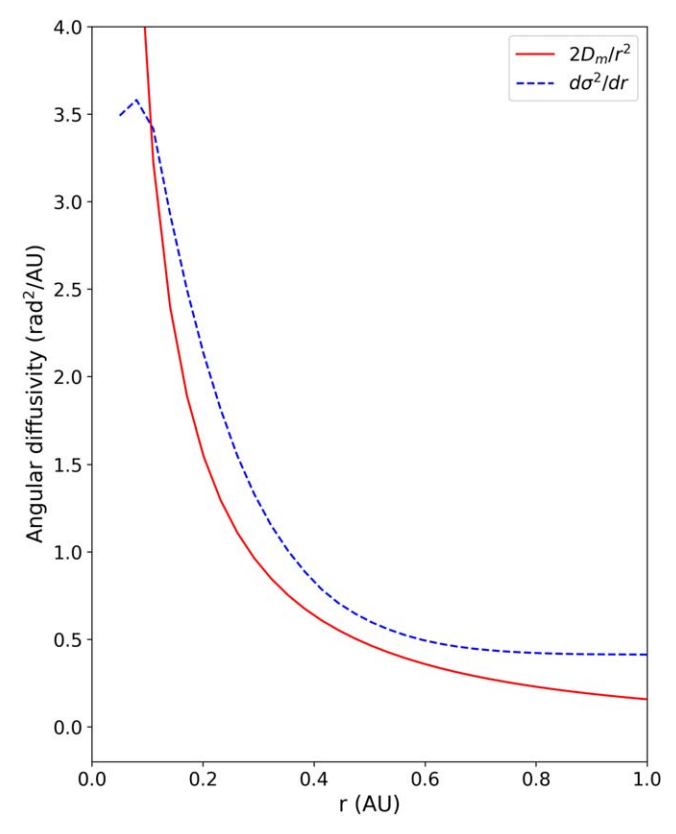


Figure 4. Numerical test of the validity of Equation (49). The radial derivative of the variance $\sigma^2(r)$ measuring the angular spread of magnetic field lines vs. twice the angular diffusivity $D_{\rm ma}(r) = D_m(r)/r^2$ is used as input in the magnetic field line transport model.

angle diffusivity and the perpendicular diffusivity, respectively. This guiding center transport equation is written in a local slab where the guiding magnetic field points in the z-direction and where the magnetic field fluctuations responsible for the diffusion of the magnetic field lines are perpendicular to the guide field direction. In this local slab model, where D is a constant,

$$\langle x(t) \rangle = \langle y(t) \rangle = 0,$$
 (51)

meaning that, on average, the guiding center position does not *drift*, as a function of time, with respect to the constant direction of the guiding magnetic field. Moreover, $z(t) = \mu vt$ when $\mu = \text{cst}$. The global scale generalization of the previous transport equation reads (Strauss & Fichtner 2015)

$$\frac{\partial f}{\partial t} + \nabla \cdot (\mu \nu \mathbf{b} f) + \frac{\partial}{\partial \mu} \left[\frac{(1 - \mu^2)}{L_B} \nu f \right]
= \frac{\partial}{\partial \mu} \left(D_{\mu\mu} \frac{\partial f}{\partial \mu} \right) + \nabla \cdot (\mathbf{D} \cdot \nabla f),$$
(52)

where b(r) is the spatially varying direction of the background magnetic field, here given by the Parker field, $L_B(r)$ is the focusing length, and D(r) is the guiding center diffusivity tensor. In this work, we have shown that the particle guiding centers experience a drift across the direction of the Parker field even in the limit where all the finite Larmor radius effects vanish.

Setting $\mu=1$ cancels all the finite Larmor radius effects 33, leaving us with an equation for the magnetic field lines. Therefore, the diffusion of stochastic Parker spirals on global heliospheric scales in the solar wind can be described by the convection–diffusion equation

$$\frac{\partial f_m}{\partial s} + \nabla \cdot (\boldsymbol{b}f_m) = \nabla \cdot (\boldsymbol{D}_m \cdot \nabla f_m), \tag{53}$$

where $f_m(\mathbf{r}, s)$ is the three-dimensional magnetic field line density distribution and $\mathbf{D}_m(\mathbf{r})$ is the magnetic field line diffusion tensor. Diffusion of the magnetic field lines is assumed to be transverse to the direction of the Parker field. Therefore, the diffusion tensor \mathbf{D}_m can be expressed in the heliographic coordinate system as

$$\boldsymbol{D}_{m} = \begin{pmatrix} D_{m}^{rr} = D_{m} \sin^{2} \chi & D_{m}^{r\theta} = 0 & D_{m}^{r\phi} = D_{m} \sin \chi \cos \chi \\ D_{m}^{\theta r} = 0 & D_{m}^{\theta \theta} = D_{m} & D_{m}^{\theta \phi} = 0 \\ D_{m}^{\phi r} = D_{m} \sin \chi \cos \chi & D_{m}^{\phi \theta} = 0 & D_{m}^{\phi \phi} = D_{m} \cos^{2} \chi, \end{pmatrix},$$

$$(54)$$

where χ is the angle between the Parker field and the radial direction. In addition to the geometrical factors depending on χ , the expression for the diffusion tensor D_m involves the local magnetic field line diffusivity D_m , a scalar that can be inferred from measurements at the spacecraft location via (Bian & Li 2022b)

$$D_m = \frac{\pi}{2} \frac{E_B(k_{\parallel} = 0)}{B_0^2},\tag{55}$$

where $E_B(k_{\parallel})$ is the spectrum of the perpendicular magnetic field fluctuations evaluated along the magnetic field lines. Thanks to the wavelet analysis of Horbury et al. (2008), Podesta (2009), Wicks et al. (2010), and others, the radial dependence of $D_m(r)$ can in principle be constrained from spacecraft measurements of $E_B(k_{\parallel})$ at various distances from the Sun. We are not aware of any direct evaluation of the local magnetic field line diffusivity via extrapolation to zero k_{\parallel} of the measured $E_B(k_{\parallel})$. For simplicity, we adopted here the model assumptions described by Strauss et al. (2017) in order to constrain from observations the radial dependence of the diffusivity $D_m(r)$. Future work could also employ outputs from turbulence transport models (see, e.g., Zank et al. 2017, 2018; Oughton & Engelbrecht 2021) to constrain the spatial dependence of the field line angular diffusivity coefficient, in an approach similar to that of, e.g., Adhikari et al. (2022). The angular diffusivity $D_{\text{ma}}(r) = D_{\text{m}}(r)/r^2$, which is used as input in the model, is plotted in Figure 4.

Expressing the magnetic field line diffusion model in the heliographic coordinate system yields

$$\frac{\partial f_{m}}{\partial s} + \frac{1}{r^{2}} \frac{\partial r^{2} \cos \chi f_{m}}{\partial r} - \frac{1}{r \sin \theta} \frac{\partial \sin \chi f_{m}}{\partial \phi} \\
= \frac{1}{r^{2}} \frac{\partial}{\partial r} r^{2} D_{m}^{rr} \frac{\partial f_{m}}{\partial r} + \frac{1}{r \sin \theta} \frac{\partial}{\partial \phi} D_{m}^{\phi r} \frac{\partial f_{m}}{\partial r} \\
+ \frac{1}{r^{2} \sin \theta} \frac{\partial}{\partial \theta} \sin \theta D_{m}^{\theta \theta} \frac{\partial f_{m}}{\partial \theta} \\
+ \frac{1}{r^{2} \sin^{2} \theta} \frac{\partial}{\partial \phi} D_{m}^{\phi \phi} \frac{\partial f_{m}}{\partial \phi} + \frac{1}{r^{2} \sin \theta} \frac{\partial}{\partial r} r D_{m}^{r\phi} \frac{\partial f_{m}}{\partial \phi}. \tag{56}$$

The heliospheric magnetic field line density distribution does not only spread in the angles θ and ϕ ; it also spreads in r owing to the radial diffusion. The radial diffusion of the magnetic field lines is the consequence of the presence of radial magnetic field fluctuations in the solar wind. The heliospheric magnetic field line distribution $f_m(\mathbf{r}, s)$ emanating from a point source at the Sun is obtained by numerically solving the drift diffusion Equation (56) in the ecliptic plane $\theta = 0$. The radial dependence of the angular distribution of the magnetic field lines is determined, showing that the field line angular distributions remain close to circular Gaussian distributions, although developing a skewness that is not described by a Gaussian model. It is also shown that in the radially evolving solar wind turbulence the magnetic field lines emanating from the Sun differ, on average, from the spirals predicted by Parker. These spirals remain Archimedean but are underwound. Our model predicts a spiral angle that is smaller by $\sim 5^{\circ}$ than the Parker spiral angle of \sim 47° at Earth's orbit for the same solar wind speed of $V_{\rm sw} = 400 \, \rm km \, s^{-1}$. It also predicts an angular position on the solar disk of the best magnetically connected footpoint to an observer at 1 au that is shifted westward by $\sim 10^{\circ}$ with respect to the Parker's model.

At first glance the result presented here of a $\sim 5^{\circ}$ underwound field relative to the standard Parker model appears to contradict the findings of Smith & Bieber (1991), who, after an analysis of 23 yr worth of hourly spacecraft observations of the heliospheric magnetic field winding angle, conclude that the observed winding angle is on average larger than expected from the standard Parker model. It should, however, be noted that the parameter choices made in the present model are applicable to solar minimum conditions. When the observations of Smith & Bieber (1991) during periods of low solar activity are considered, it can be seen from Figure 2 of that study that the observed winding angle is actually several degrees smaller than the nominal Parker value, thereby providing a possible observational confirmation of our analysis. Subsequent studies, although providing confirmation of the solar-cycle-dependent behavior of the winding angle, report values closer to the nominal Parker angle during solar minimum periods (e.g., Hanneson et al. 2020; Chang et al. 2022). Nevertheless, our results are consistent with the recent analysis by Fargette et al. (2021) showing that as the Parker Solar Probe's distance to the Sun decreases, the magnetic field directional data of the quiet solar wind deviate, on average, from the Parker spiral model predictions. The spiral is observed to be less tightly wound than predicted by Parker on the basis of the measurements of the radial solar wind speed processed with a 2 hr low-pass filter.

The magnetic field line density distributions displayed in Figure 1 can equivalently be interpreted as the density distributions of particle guiding centers, electrons and ions, promptly injected from the solar source and propagating ballistically with a constant pitch angle along the diffusing magnetic field lines. The four different panels in Figure 1 thus correspond to four different times after injection at the Sun. Moreover, the magnetic field line density distribution displayed in Figure 2 can equivalently be interpreted as a steady-state density distribution of particles injected at the solar source, under scatter-free conditions. The above results show that, due to solar wind turbulence, the average guiding center trajectory drifts westward, from the nominal Parker field line it emanates

from at the Sun, by an amount of the order of $\sim \! 10^{\circ}$ at 1 au. Therefore, the presence of turbulence can significantly change the angle of best magnetic connection between possible sources of particle acceleration at the Sun and observers of SEP events in the inner heliosphere. These results are the most pertinent to the transport of scatter-free electrons (Lin 1974) accelerated during solar flares.

We have shown that a substantial amount of radial broadening of the particle density distributions can be attributed to the radial diffusion of the magnetic field lines alone, without the need to invoke the role of pitch-angle scattering in order to explain it. Pitch-angle scattering produces radial diffusion of the emitted particles, which affects the timing of their arrival at the observer's position. Radial diffusion of the magnetic field lines thus constitutes an additional source of interpretations of the results obtained from velocity dispersion analysis applied to the onset time of SEP events (Lin 1974). While the terms responsible for pitch-angle diffusion and cross-field diffusion are easily distinguished in transport models, disentangling their roles in the transport of the fast particles is a more complicated task. This is the reason we have based our analysis on the idealized case of scatter-free transport along stochastic magnetic field lines, i.e., we focused on the global structure of the stochastic magnetic field lines in the heliosphere. Disentangling the role of magnetic field line diffusion from that of pitch-angle scattering in the transport of SEPs will be the subject of forthcoming investigations. A specific question we are interested in answering is, can the finite Larmor radius effect of turbulent pitch-angle scattering increase the amount of angular spread of the SEPs with respect to that of the dispersing magnetic field lines, say, at 1 au, by increasing the time spent by the particles between the emission region and the observer position? The three-dimensional particle transport model suggests that pitch-angle scattering may decouple the particle paths from the magnetic field lines. This property cannot emerge from one-dimensional fieldaligned transport models, where the particles are tied to a given meandering magnetic field line. If pitch-angle scattering can decouple the particle paths from the magnetic field lines, it remains to evaluate in which amounts in the three-dimensional model. An important observational constraint is that the angular spreads of the particles do not depend substantially on the charge-to-mass ratio (Cohen et al. 2017).

Acknowledgments

This work is supported in part by NASA grants 80NSSC19K0075, 80NSSC21K1327, and 80NSSC21K1814 and NSF ANSWERS 2149771. G.L. and N.B. acknowledge support through ISSI team 581.

ORCID iDs

N. H. Bian https://orcid.org/0000-0003-0142-8669
R. D. Strauss https://orcid.org/0000-0002-0205-0808
G. Li https://orcid.org/0000-0003-4695-8866
N. E. Engelbrecht https://orcid.org/0000-0003-3659-7956

References

Adhikari, L., Zank, G. P., Telloni, D., & Zhao, L. L. 2022, ApJL, 937, L29 Antiochos, S. K. 1987, ApJ, 312, 886
Belcher, J. W., & Davis, L. J. 1971, JGR, 76, 3534
Berger, M. A. 1988, A&A, 201, 355
Bian, N. H., & Emslie, A. G. 2019, ApJ, 880, 11

```
Bian, N. H., & Emslie, A. G. 2020, ApJ, 897, 34
Bian, N. H., Kontar, E. P., & MacKinnon, A. L. 2011, A&A, 535, A18
Bian, N. H., & Li, G. 2021, ApJ, 908, 45
Bian, N. H., & Li, G. 2022a, ApJ, 924, 120
Bian, N. H., & Li, G. 2022b, ApJ, 941, 58
Boldyrev, S. 2006, PhRvL, 96, 115002
Burger, R. A., Krüger, T. P. J., Hitge, M., & Engelbrecht, N. E. 2008, ApJ,
Burger, R. A., Nel, A. E., & Engelbrecht, N. E. 2022, ApJ, 926, 128
Cane, H. V., McGuire, R. E., & von Rosenvinge, T. T. 1986, ApJ, 301, 448
Cary, J. R., & Littlejohn, R. G. 1983, AnPhy, 151, 1
Chandrasekhar, S. 1943, RvMP, 15, 1
Chang, Q., Xu, X., Wang, X., et al. 2022, ApJ, 931, 105
Cherstvy, A. G., Chechkin, A. V., & Metzler, R. 2013, NJPh, 15, 083039
Cliver, E. W. 2000, in AIP Conf. Proc. 528, ACE 2000 Symp. (Melville, NY:
   AIP), 21
Cohen, C. M. S., Mason, G. M., & Mewaldt, R. A. 2017, ApJ, 843, 132
Corrsin, S. 1959, AdGeo, 6, 161
Dalla, S., Balogh, A., Krucker, S., et al. 2003, GeoRL, 30, 8035
Dresing, N., Gómez-Herrero, R., Heber, B., et al. 2014, A&A, 567, A27
Dröge, W., Kartavykh, Y. Y., Dresing, N., Heber, B., & Klassen, A. 2014,
   JGRA, 119, 6074
Dudok de Wit, T., Krasnoselskikh, V. V., Bale, S. D., et al. 2020, ApJS,
  246, 39
Earl, J. A. 1976, ApJ, 205, 900
Elsasser, K. 1986, PPCF, 28, 1743
Engelbrecht, N. E., & Burger, R. A. 2015, ApJ, 814, 152
Engelbrecht, N. E., & Wolmarans, C. P. 2020, AdSpR, 66, 2722
Eyink, G. L., Lazarian, A., & Vishniac, E. T. 2011, ApJ, 743, 51
Fan, C. Y., Pick, M., Pyle, R., Simpson, J. A., & Smith, D. R. 1968, JGR,
   73, 1555
Fargette, N., Lavraud, B., Rouillard, A. P., et al. 2021, ApJ, 919, 96
Fermi, E. 1949, PhRv, 75, 1169
Feynman, R. P. 1963, in Feynman Lectures on Physics, ed. R. P. Feynman,
   R. B. Leighton, & M. Sands, Vol. 1 (Reading, MA: Addison-Wesley)
Fisk, L. A. 1996, JGR, 101, 15547
Fisk, L. A. 2001, JGR, 106, 15849
Goldreich, P., & Sridhar, S. 1995, ApJ, 438, 763
Hanneson, C., Johnson, C. L., Mittelholz, A., Al Asad, M. M., & Goldblatt, C.
   2020, JGRA, 125, e27139
Horbury, T. S., Forman, M., & Oughton, S. 2008, PhRvL, 101, 175005
Jokipii, J. R. 1966, ApJ, 146, 480
Jokipii, J. R., & Parker, E. N. 1969, ApJ, 155, 777
Kontar, E. P., Hannah, I. G., & Bian, N. H. 2011, ApJL, 730, L22
Krucker, S., & Lin, R. P. 2000, ApJL, 542, L61
Lario, D., Kallenrode, M. B., Decker, R. B., et al. 2006, ApJ, 653, 1531
Leighton, R. B. 1964, ApJ, 140, 1547
Li, B., Cairns, I. H., Gosling, J. T., et al. 2016, JGRA, 121, 925
Lin, R. P. 1974, SSRv, 16, 189
Litvinenko, Y. E. 2012, ApJ, 745, 62
Longcope, D. W. 2005, LRSP, 2, 7
Lorenz, E. N. 1963, JAtS, 20, 130
Matthaeus, W. H., Bieber, J. W., Ruffolo, D., Chuychai, P., & Minnie, J. 2007,
   ApJ, 667, 956
```

```
Matthaeus, W. H., Gray, P. C., Pontius, D. H. J., & Bieber, J. W. 1995, PhRvL,
  75, 2136
McComas, D. J., Christian, E. R., Cohen, C. M. S., et al. 2019, Natur, 576, 223
Mewaldt, R. A., Cohen, C. M. S., Mason, G. M., et al. 2013, in AIP Conf. Ser.
  1539, Solar Wind 13, ed. G. P. Zank et al. (Melville, NY: AIP), 116
Meyer, P., Parker, E. N., & Simpson, J. A. 1956, PhRv, 104, 768
Moradi, A., & Li, G. 2019, ApJ, 887, 102
Morozov, A. I., & Solov'ev, L. S. 1966, RvPP, 2, 1
Morrison, P. J. 2000, PhPl, 7, 2279
Nolte, J. T., & Roelof, E. C. 1973, SoPh, 33, 241
Oughton, S., & Engelbrecht, N. E. 2021, NewA, 83, 101507
Oughton, S., Matthaeus, W. H., Wan, M., & Osman, K. T. 2015, RSPTA, 373,
  20140152
Owens, M. J., & Forsyth, R. J. 2013, LRSP, 10, 5
Parker, E. N. 1958, ApJ, 128, 664
Parker, E. N., & Tidman, D. A. 1958, PhRv, 111, 1206
Podesta, J. J. 2009, ApJ, 698, 986
Reames, D. V. 1999, SSRv, 90, 413
Reames, D. V., Ng, C. K., & Tylka, A. J. 2013, SoPh, 285, 233
Richardson, I. G., von Rosenvinge, T. T., Cane, H. V., et al. 2014, SoPh,
   289, 3059
Rodríguez-Pacheco, J., Wimmer-Schweingruber, R. F., Mason, G. M., et al.
  2020, A&A, 642, A7
Roelof, E. C. 1969, in Lectures in High-Energy Astrophysics, ed.
  H. Ögelman & J. R. Wayland (Washington, DC: NASA), 111
Sáiz, A., Evenson, P., Ruffolo, D., & Bieber, J. W. 2005, ApJ, 626, 1131
Schatten, K. H., Ness, N. F., & Wilcox, J. M. 1968, SoPh, 5, 240
Schekochihin, A. A., Cowley, S. C., Dorland, W., et al. 2009, ApJS, 182,
Shea, M. A., & Smart, D. F. 1990, SoPh, 127, 297
Smith, C. W., & Bieber, J. W. 1991, ApJ, 370, 435
Strauss, R. D., & Fichtner, H. 2015, ApJ, 801, 29
Strauss, R. D., & le Roux, J. A. 2019, ApJ, 872, 125
Strauss, R. D. T., Dresing, N., & Engelbrecht, N. E. 2017, ApJ, 837, 43
Tylka, A. J., Cohen, C. M. S., Dietrich, W. F., et al. 2003, ICRC (Tsukuba),
  6, 3305
Van Hollebeke, M. A. I., Ma Sung, L. S., & McDonald, F. B. 1975, SoPh,
  41, 189
Wang, L., Krucker, S., Mason, G. M., Lin, R. P., & Li, G. 2016, A&A,
  585, A119
Wang, L., Lin, R. P., & Krucker, S. 2011, ApJ, 727, 121
Wicks, R. T., Horbury, T. S., Chen, C. H. K., & Schekochihin, A. A. 2010,
   MNRAS, 407, L31
Wiedenbeck, M. E., Mason, G. M., Cohen, C. M. S., et al. 2013, ApJ, 762,
Yeates, A. R., & Hornig, G. 2016, A&A, 594, A98
Zank, G. P., Adhikari, L., Hunana, P., et al. 2017, ApJ, 835, 147
Zank, G. P., Adhikari, L., Hunana, P., et al. 2018, ApJ, 854, 32
Zhang, M., McKibben, R. B., Lopate, C., et al. 2001, ICRC (Hamburg),
  8, 3302
Zhang, M., McKibben, R. B., Lopate, C., et al. 2003, JGRA, 108, 1154
Zhao, L., Li, G., Zhang, M., et al. 2019, ApJ, 878, 107
Zhao, L. L., Adhikari, L., Zank, G. P., Hu, Q., & Feng, X. S. 2018, ApJ,
   856, 94
```